

# Direct synthesis of extra-heavy olefins from carbon monoxide and water

Received: 16 September 2022

Accepted: 21 March 2023

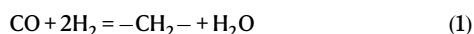
Published online: 03 April 2023

 Check for updates

 Chuanhao Wang<sup>1,3</sup>, Junjie Du<sup>1,3</sup>, Lin Zeng<sup>1</sup>, Zhongling Li<sup>1</sup>, Yizhou Dai<sup>1</sup>, Xu Li<sup>1</sup>, Zijun Peng<sup>1</sup>, Wenlong Wu<sup>1</sup>, Hongliang Li<sup>1</sup> & Jie Zeng<sup>1,2</sup>

Extra-heavy olefins ( $C_{12+}$ ), feedstocks to synthesize a wide range of value-added products, are conventionally generated from fossil resources *via* energy-intensive wax cracking or multi-step processes. Fischer-Tropsch synthesis with sustainably obtained syngas as feed-in provides a potential way to produce  $C_{12+}$ , though there is a trade-off between enhancing C-C coupling and suppressing further hydrogenation of olefins. Herein, we achieve selective production of  $C_{12+}$  *via* the overall conversion of CO and water, denoted as Kölbel-Engelhardt synthesis (KES), in polyethylene glycol (PEG) over a mixture of Pt/Mo<sub>2</sub>N and Ru particles. KES provides a continuously high CO/H<sub>2</sub> ratio, thermodynamically favoring chain propagation and olefin formation. PEG serves as a selective extraction agent to hinder hydrogenation of olefins. Under an optimal condition, the yield ratio of CO<sub>2</sub> to hydrocarbons reaches the theoretical minimum, and the  $C_{12+}$  yield reaches its maximum of 1.79 mmol with a selectivity (among hydrocarbons) of as high as 40.4%.

Extra-heavy olefins ( $C_{12+}$ ), production of which are highly relative to fossil energy with energy-intensive processes, are extensively used as feedstocks to synthesize a wide range of value-added products such as synthetic lubricants, surfactants, sizing agents, drilling fluid, biodegradable detergents, new polymers, and plasticizers<sup>1,2</sup>. Conventionally,  $C_{12+}$  are produced from energy-intensive wax cracking<sup>3</sup> or multi-step Shell higher olefin process (SHOP) containing oligomerization, isomerization, and metathesis with ethylene as original feedstock<sup>2</sup>. The ever-increasing depletion of petroleum reserves is spurring the exploration of sustainable production routes from non-petroleum carbon resources. Fischer-Tropsch synthesis (FTS) offers an approach to produce hydrocarbons such as light olefins, aromatics, gasoline, and diesel directly from syngas which readily derives from coal, biomass, CO<sub>2</sub>, and natural gas (Eq. 1)<sup>4–8</sup>.

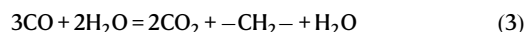


However, under classic FTS conditions, there is a trade-off between enhancing C-C coupling for long-chain products ( $C_{12+}$ ) and suppressing further hydrogenation of olefins. For instance, though iron nanoparticles on  $\alpha$ -alumina<sup>8</sup>, cobalt carbide nanoprisms<sup>9</sup>, and Oxide-Zeolite<sup>10</sup> favored the formation of olefins, these catalysts exhibited limiting selectivity for  $C_{12+}$  products. For ruthenium (Ru)-based catalysts with intrinsically high activity for chain growth<sup>11–13</sup>, most of the produced long-chain hydrocarbons are paraffins instead of olefins<sup>14</sup>, because Ru is highly active for the hydrogenation of unsaturated hydrocarbons. Though efforts have been devoted to the production of  $C_{12+}$  in a few case studies<sup>15,16</sup>, it is of a grand challenge to propose a universal strategy to massively synthesize  $C_{12+}$ .

To break this counterbalance, we propose an alternative reaction route, Kölbel-Engelhardt synthesis (KES), which is the coupling of the water gas shift (WGS) reaction (Eq. 2) and FTS (Eq. 1). This cascade reaction (Eq. 3) was proposed in last century to utilize the CO-rich syngas, though it was not widely recognized in the field of CO conversion,

<sup>1</sup>Hefei National Research Center for Physical Sciences at the Microscale, Key Laboratory of Strongly-Coupled Quantum Matter Physics of Chinese Academy of Sciences, Key Laboratory of Surface and Interface Chemistry and Energy Catalysis of Anhui Higher Education Institutes, Department of Chemical Physics, University of Science and Technology of China, 230026 Hefei, Anhui, P. R. China. <sup>2</sup>School of Chemistry & Chemical Engineering, Anhui University of Technology, 243002 Ma'anshan, Anhui, P. R. China. <sup>3</sup>These authors contributed equally: Chuanhao Wang, Junjie Du. ✉ e-mail: [lihl@ustc.edu.cn](mailto:lihl@ustc.edu.cn); [zengj@ustc.edu.cn](mailto:zengj@ustc.edu.cn)

not to mention practically replacing the unit of WGS and FTS, considering excess CO<sub>2</sub> production and inhibited chain propagation<sup>17–19</sup>. Xu et al. reported the feasibility of this process in a slurry reactor over Ru-based catalysts, and considerable chain propagation was achieved, though a large margin still existed, in terms of CO<sub>2</sub> excess or inadequate C<sub>5+</sub> production compared with conventional FTS<sup>20</sup>.



Herein, we achieved highly selective production of C<sub>12+</sub><sup>+</sup> *via* direct conversion of CO and stoichiometric water (KES) in the solvent of polyethylene glycol (PEG) over Ru-based catalysts. During the cascade reaction of WGS and FTS, the sustained release of hydrogen *via* WGS afforded continuously low hydrogen pressure which kinetically benefited both chain propagation and olefin formation during FTS. The phase-transfer agent, PEG, served as a selective extraction agent to increase the selectivity for olefins. A mixture of Pt/Mo<sub>2</sub>N and Ru particles, which served as active components for WGS and FTS, respectively, was applied as the catalyst. In PEG under 2 MPa of CO with a stoichiometric ratio (3:2) of CO:H<sub>2</sub>O at 200 °C for 10 h, the yield ratio of CO<sub>2</sub> to hydrocarbons reached the theoretical minimum of 2 (Eq. 3), reflecting the perfect kinetic match of WGS and FTS. Moreover, the C<sub>12+</sub><sup>+</sup> yield reached its maximum of 1.79 mmol with a selectivity (among hydrocarbons) of as high as 40.4%. Universality was also studied by replacing the noble-meta-containing catalysts to noble-metal-free catalysts.

## Results

### Characterizations of KES catalysts

To validate the effectiveness of KES, we prepared a catalyst consisting of active components for WGS and FTS. Specifically, Pt/Mo<sub>2</sub>N was fabricated for WGS, since Mo-based materials have already been

reported to dissociate water molecules at a relatively low temperature (-150 °C)<sup>21–23</sup>. Mo<sub>2</sub>N, instead of molybdenum carbides, was chosen to avoid carbon contamination. The mass loading of Pt was determined to be 2.0% according to inductively coupled plasma-atomic emission spectrometry (ICP-AES). This mass loading was reported active with the capability of stabilizing Mo-based surface by rapid consumption of oxygen species from water dissociation in WGS process<sup>23</sup>. Such a low mass loading accounted for the absence of diffraction peaks of Pt in the X-ray diffraction spectroscopy (XRD) patterns of Pt/Mo<sub>2</sub>N (Supplementary Fig. S1). The high-angle annular dark-field scanning transmission electron microscopy (HAADF-STEM) image of Pt/Mo<sub>2</sub>N showed that Pt particles with a main size of ~2.5 nm were densely deposited on the support (Supplementary Fig. S2). This dense distribution ensured the rapid reaction of oxygen species with CO\* on Pt to avoid the oxidation of Mo<sub>2</sub>N<sup>23</sup>. For the production of C<sub>12+</sub><sup>+</sup>, FTS catalyst was set to Ru particles due to its outstanding activity for the chain propagation<sup>11–13</sup>.

The mixture of Pt/Mo<sub>2</sub>N and Ru particles, denoted as Pt/Mo<sub>2</sub>N-Ru, was used as the catalyst for KES. In a typical synthesis of Pt/Mo<sub>2</sub>N-Ru, RuCl<sub>3</sub>·xH<sub>2</sub>O, and Pt/Mo<sub>2</sub>N were dispersed in a reactor containing a mixture of PEG and water. Afterwards, the reactor was pressurized with hydrogen and heated to obtain Ru particles before the formal catalytic tests. As shown in the XRD patterns, a distinct set of peaks for Mo<sub>2</sub>N and a broad set of peaks for metallic Ru appeared (Fig. 1a). Figure 1b–f shows X-ray photoelectron spectroscopy (XPS) spectra of Pt/Mo<sub>2</sub>N-Ru. The presence of Mo<sup>6+</sup> and Mo<sup>4+</sup> was ascribed to inevitable surface oxidation during passivation in CO<sub>2</sub> atmosphere (Fig. 1b, c)<sup>24</sup>. The C 1s spectrum exhibited a peak at 286.3 eV which was assigned to the PEG residual on the surfaces of the catalyst (Fig. 1d). Based on Ru 3d, Ru 3p, Ru 4s, and Pt 4f spectra, both Ru and Pt were identified in metallic states (Fig. 1d–f). Notably, the Ru 3d<sub>5/2</sub> peak located at 280.4 eV suggested negligible electronic interaction between PEG and Ru particles<sup>25</sup>. Supplementary Figure S3 shows scanning transmission electron microscopy-energy diffraction X-ray (STEM-EDX) elemental

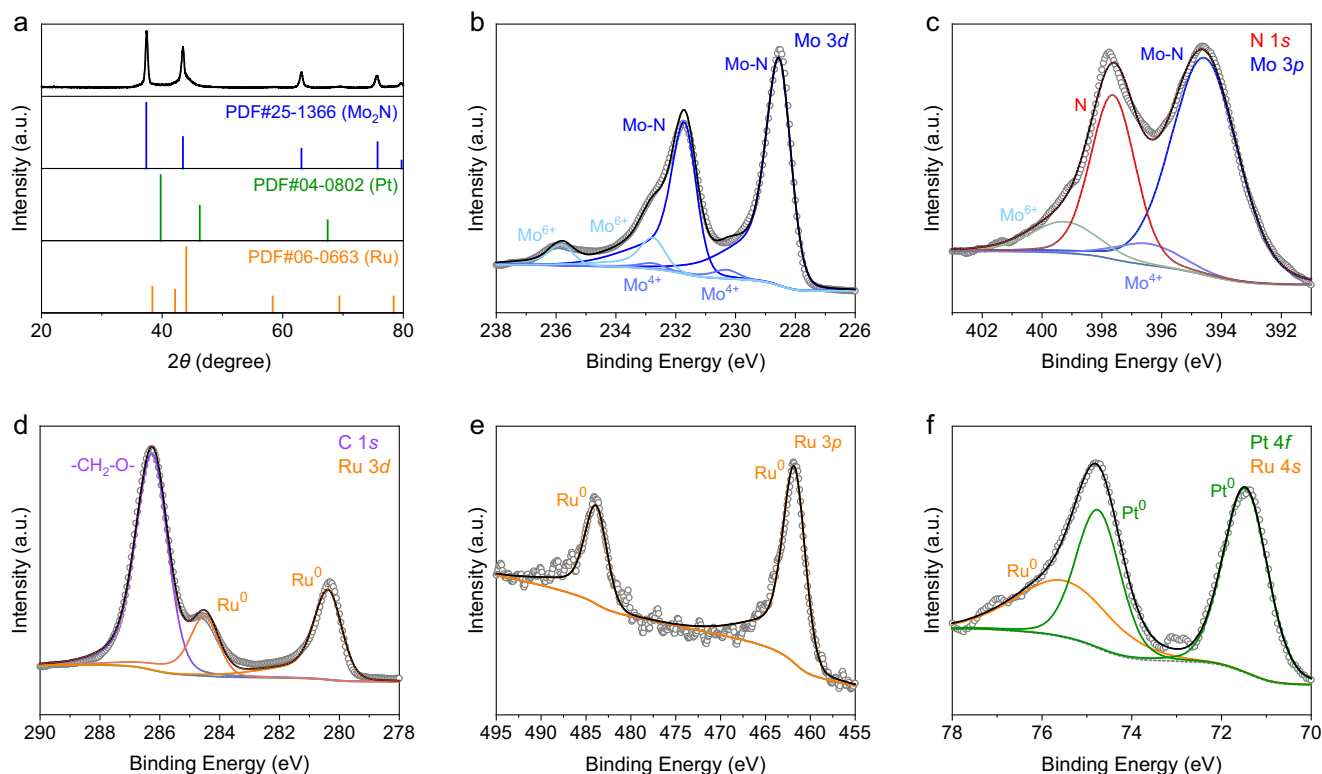


**Fig. 1 | Structural characterizations of Pt/Mo<sub>2</sub>N-Ru.** **a** XRD pattern of Pt/Mo<sub>2</sub>N-Ru. **b** Mo 3d, **c** N 1s and Mo 3p, **d** C 1s and Ru 3d, **e** Ru 3p, and **f** Pt 4f and Ru 4s XPS spectra of Pt/Mo<sub>2</sub>N-Ru.

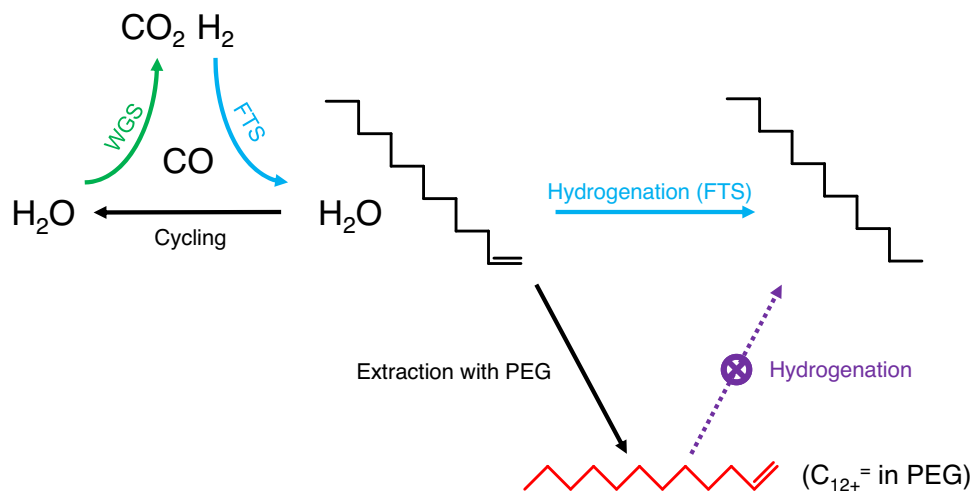


**Fig. 2 | Scheme of sustained release of hydrogen *via* KES and selective extraction to promote the production of extra-heavy olefins.** The green arrow represents WGS. The azure arrows represent FTS, containing chain propagation and hydrogenation. The dark violet arrow represents hydrogenation of dissolved olefins. For KES, hydrogen accumulates through WGS and is gradually consumed

through FTS. Water by-produced from FTS serves again as reactant of WGS. Hence a relatively high CO/H<sub>2</sub> ratio, which thermodynamically favors the production of C<sub>12+</sub>, is maintained. Besides, a phase-transfer agent (PEG) with an affinity to olefins extracts olefin intermediates from surfaces of FTS catalysts to inhibit their further hydrogenation.

mapping images of Pt/Mo<sub>2</sub>N-Ru. We observed different distribution pattern of Ru from those of Mo, N, and Pt, suggesting that Ru particles were not supported on Pt/Mo<sub>2</sub>N. This was attributed to the capping effect of PEG, as reported elsewhere<sup>26</sup>. These small particles could have abundant step sites for CO activation<sup>27</sup>. For comparison, Ru deposited on Pt/Mo<sub>2</sub>N was also prepared, denoted as Ru/Pt/Mo<sub>2</sub>N, to verify the significance of the separation of Ru and Pt/Mo<sub>2</sub>N. EDX mapping of Ru/Pt/Mo<sub>2</sub>N indicated that Ru particles were mainly supported on Pt/Mo<sub>2</sub>N (Supplementary Fig. S4).

### Catalytic properties of Pt/Mo<sub>2</sub>N-Ru towards KES

Despite hydrogen being invisible at both sides of Eq. (3), kinetically, hydrogen produced from WGS is necessary to drive FTS. Excess CO<sub>2</sub> production reported before also suggested the difficulty to achieve this ideal condition. Though, different from a constant CO/H<sub>2</sub> ratio in conventional FTS, in KES conducted in a slurry reactor hydrogen is sustainably released from WGS and gradually consumed in FTS. This should provide a relatively high CO/H<sub>2</sub> ratio, which favors chain propagation and suppresses the further hydrogenation of olefins. With this condition thermodynamically favorable for the production of C<sub>12+</sub>, we still need the kinetic feasibility. Various solvents were applied when FTS was conducted in slurry reactors<sup>28</sup>. Phase-transfer agents exhibit affinity to both polar phases and non-polar phases<sup>29</sup>. PEG is one of the most widely used phase-transfer agents<sup>30</sup>. The characteristic affinity to organic compounds inspired us to explore the possibility of stabilizing olefins formed on the surfaces of catalysts. Hence, we first investigated the interaction between PEG and olefin. With cyclohexane as the extraction agent, 87% of 1-dodecene was extracted from PEG (PEG-400, unless mentioned specifically) (Supplementary Fig. S5). With the aid of a more polar solvent, water, this residue of 1-dodecene was completely expelled into cyclohexane solution, leading to an extraction efficiency of >99%. This contrast indicated a measurable interaction between PEG and olefins. As such, we assumed that PEG could potentially serve as an extractor for olefin intermediates formed during KES (Fig. 2).

The catalytic tests were conducted over constant amounts of Pt/Mo<sub>2</sub>N-Ru in a mixture of PEG and water under different pressures of CO at 200 °C for 10 h, denoted as the standard condition. In this condition, the amount of water was tuned to keep the molar ratio of CO to H<sub>2</sub>O at 3/2 (Eq. 3), while the total volume of binary PEG/water solvent was kept to 15 mL. Notably, the oxygenate products were below the detection limit of gas chromatography (GC). When the

pressure of CO increased from 2 MPa to 4 MPa, the yield of CO<sub>2</sub> underwent a steady increase from 8.63 to 30.46 mmol under the standard condition (Fig. 3a, Supplementary Table S1), as expected from the volume contraction character of KES. In contrast, hydrocarbon production exhibited a saddle-shaped trend with the increasing pressure, along with the amount of water. Specially, the yield of hydrocarbons reached the minimum of 3.43 mmol under 3 MPa of CO, whereas the yields were 4.42 and 5.81 mmol under 2 and 4 MPa, respectively (Fig. 3a, Supplementary Table S1). As a result, the ratio of CO<sub>2</sub> to hydrocarbons continuously raised with the elevated pressure of CO (Fig. 3a). It was worth noting that the ratio of 1.95 obtained under 2 MPa of CO was close to the stoichiometric CO<sub>2</sub>/–CH<sub>2</sub>– ratio of 2:1 as stated in Eq. (3). This result indicated the perfect match of WGS and FTS under specific condition. For hydrocarbon yield, the promotion effect of pressurization observed in conventional FTS process was absent here. The chain propagation was also inhibited at elevated pressures from the perspective of decreasing C<sub>5+</sub> selectivity of 88.5% (2 MPa), 84.6% (3 MPa), and 67.4% (4 MPa) (Fig. 3b). This was quite different from FTS process at elevated pressures where CO\* coverage was increased and thus more CH<sub>x</sub>\* generated. We speculated this abnormal pressurization effect came from relatively sluggish kinetics of FTS, in consideration of all necessary hydrogen for FTS, a reaction of gaseous components, was produced *via* WGS, a reaction of a gaseous component and a dissolved component. CO diffusing into PEG phase were prone to directly react with OH\* adsorbed on Pt/Mo<sub>2</sub>N instead of dissociating on the surface of Ru and waiting for diffusing hydrogen to form CH<sub>x</sub>.

It is worth noting that olefins took the dominance of hydrocarbon production, which contrasted both the major production of paraffins over undecorated Ru-based catalysts reported before<sup>14</sup> and a higher temperature demanded for olefin production<sup>4,10</sup>. Detailed hydrocarbon distribution suggested chain propagation under 3 MPa of CO was similar to that under 2 MPa (Fig. 3c, Supplementary Fig. S6a), while 4 MPa of CO severely suppressed chain propagation (Supplementary Fig. S6b). We also observed that the ratio of olefins to paraffins among all C<sub>2+</sub> products (o/p ratio) exhibited a positive relationship with the pressure of CO, whereas the selectivity for C<sub>12+</sub> hydrocarbons took an opposite tendency (Fig. 3b). Although the selectivity for C<sub>12+</sub> among hydrocarbons under 2 MPa was 40.4%, slightly lower than that (41.9%) under 3 MPa, the C<sub>12+</sub> yield was optimized at 1.79 mmol under 2 MPa with other reaction parameters keeping the same as this standard

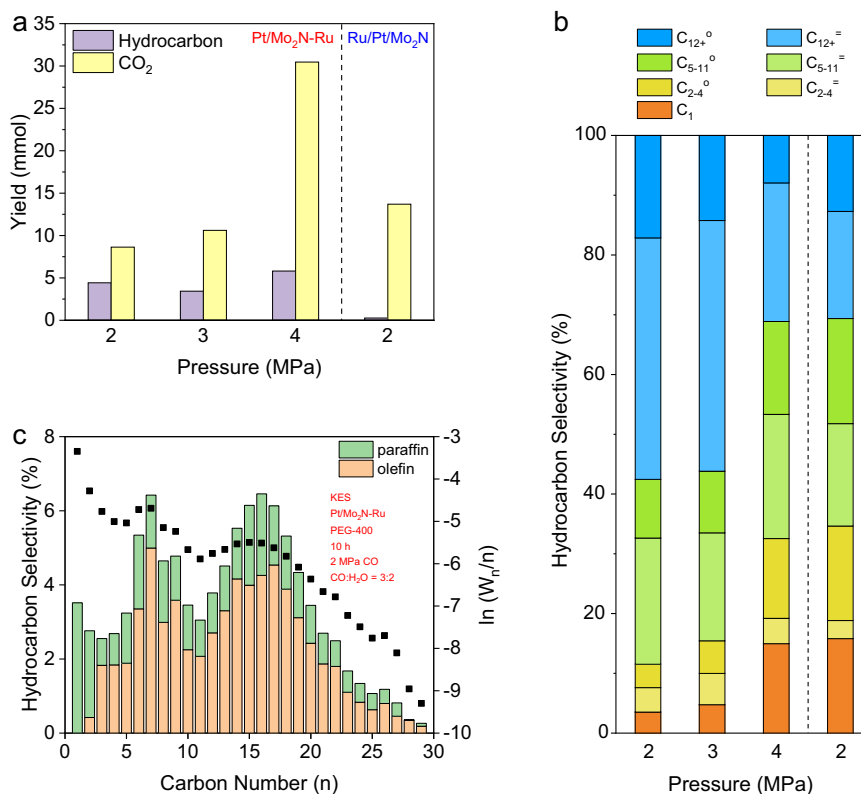


**Fig. 3 | Catalytic performances of KES. a** Yields of hydrocarbons and CO<sub>2</sub> on a carbon-atom basis. From left to right: 2, 3, and 4 MPa of CO over Pt/Mo<sub>2</sub>N-Ru, and 2 MPa of CO over Ru/Pt/Mo<sub>2</sub>N. **b** Fractional hydrocarbon selectivity. From left to right: 2, 3, and 4 MPa of CO over Pt/Mo<sub>2</sub>N-Ru, and 2 MPa of CO over Ru/Pt/Mo<sub>2</sub>N. = represents olefins and o represents paraffins. **c** Detailed hydrocarbon selectivity over

Pt/Mo<sub>2</sub>N-Ru under 2 MPa of CO. All catalytic experiments were conducted in a 50-ml Hastelloy slurry reactor at 200 °C for 10 h with a CO:H<sub>2</sub>O ratio of 3:2. Total volume of PEG solvent (with 284, 426, and 568 μL of water for 2, 3, and 4 MPa of CO) were kept to 15 mL. Pt/Mo<sub>2</sub>N-Ru contained 100 mg of Pt/Mo<sub>2</sub>N and -37 mg of Ru particles, while 137 mg of Ru/Pt/Mo<sub>2</sub>N was used to ensure the same amounts of active components.

condition (Fig. 3b, Supplementary Table S1). Thus, we denoted 2 MPa of CO along with a CO:H<sub>2</sub>O of 3:2 as the optimal condition.

The matching degree of cascade reactions can also be adjusted by the intimacy of bifunctional components<sup>31</sup>. To this end, we explored the catalytic performance of Ru/Pt/Mo<sub>2</sub>N under the optimal condition (2 MPa of CO, CO:H<sub>2</sub>O = 3:2, 200 °C, 10 h). The CO<sub>2</sub> yield increased to 13.70 mmol, while hydrocarbon production was severely suppressed with a yield of 0.27 mmol in comparison with the results over Pt/Mo<sub>2</sub>N-Ru (Fig. 3a, Supplementary Table S1). Considering that the majority of Ru was deposited on the surface of Mo<sub>2</sub>N, hydroxyl radicals generated on Mo<sub>2</sub>N *via* water dissociation reacted rapidly with CO adsorbed on Ru particles which behaved similarly to the supported Pt particles<sup>21,23</sup>. Hence, only a small fraction of CO\* participated in the FTS process, resulting in a low yield of hydrocarbons. As a result of the mismatch of WGS and FTS, the hydrogen partial pressure over Ru/Pt/Mo<sub>2</sub>N became higher than that over Pt/Mo<sub>2</sub>N-Ru, disfavoring the formation of C<sub>12+</sub><sup>=</sup>. As expected, the C<sub>12+</sub><sup>=</sup> selectivity (among hydrocarbons) of Ru/Pt/Mo<sub>2</sub>N was 17.9%, lower than that (40.4%) of Pt/Mo<sub>2</sub>N-Ru (Fig. 3b, Supplementary Fig. S7, Supplementary Table S1). Without regard to the detailed difference, the fractional hydrocarbon distribution over Ru/Pt/Mo<sub>2</sub>N under 2 MPa of CO was similar to that over Pt/Mo<sub>2</sub>N-Ru under 4 MPa of CO (Fig. 3b), suggesting the insufficiency of CO\* over Ru particles under 4 MPa of CO.

### Mechanistic studies on KES to C<sub>12+</sub><sup>=</sup>

FTS experiments with syngas as feed-in were conducted to verify our assumption and speculation. Ru particles themselves with a main size of ~2.8 nm were fabricated with the same procedure for FTS tests (Supplementary Figs. S8 and S9). Under a conventional FTS gaseous condition (CO:H<sub>2</sub> = 1:2) at 200 °C in different solvents (water and PEG), Ru

particles exhibited different hydrocarbon selectivity in water and PEG (Fig. 4b, Supplementary Fig. S10, Supplementary Table S2), while the yields of CO<sub>2</sub> and hydrocarbons were similar (Fig. 4a). Compared with the dominant production of paraffins in water, the use of PEG solvent did induce the formation of olefins with an o/p ratio of 0.92 (Supplementary Fig. S10), verifying our assumption that PEG could serve as an extractor and inhibit further hydrogenation of olefins. Difference of hydrocarbon distribution in PEG and water was also observed. Methane became the major product when water was used while a wide distribution was achieved in PEG (Supplementary Fig. S8c). We deduced that the polar character of water expelled CH<sub>x</sub> intermediates on Ru surfaces, leading to a restricted chain distribution. When we turned the CO/H<sub>2</sub> ratio from 1/2, a stoichiometric ratio for the FTS reaction (Eq. 1), to an extreme value of 9/1, the o/p ratio increased to 2.17 (Supplementary Fig. S8a, b, Supplementary Table S2), which was pretty close to that of KES under 2 MPa of CO (Supplementary Table S1). To investigate the possible CO-insertion mechanism for the chain growth, we conducted propylene hydroformylation over Ru particles in PEG. Unlike typical hydroformylation catalysts such as Rh, Ru particles exhibited an FTS-style behavior (Supplementary Fig. S11), while the oxygenates were still below the detection limit of GC. Therefore, the hydroformylation result, which fitted well with the absence of oxygenates in KES products, was not contradictory with the carbide mechanism which Ru-based catalysts preferred during FTS<sup>32-34</sup>. From FTS results, we concluded that maintaining a relatively high CO/H<sub>2</sub> ratio with PEG as the solvent could induce the formation of olefins.

WGS directly affected the CO/H<sub>2</sub> ratio, compared with hydrogen-consuming FTS which underwent sluggish diffusion of gaseous hydrogen to surfaces of Ru and activation on Ru. Hence, we should study the influence of water to the production of C<sub>12+</sub><sup>=</sup>. In

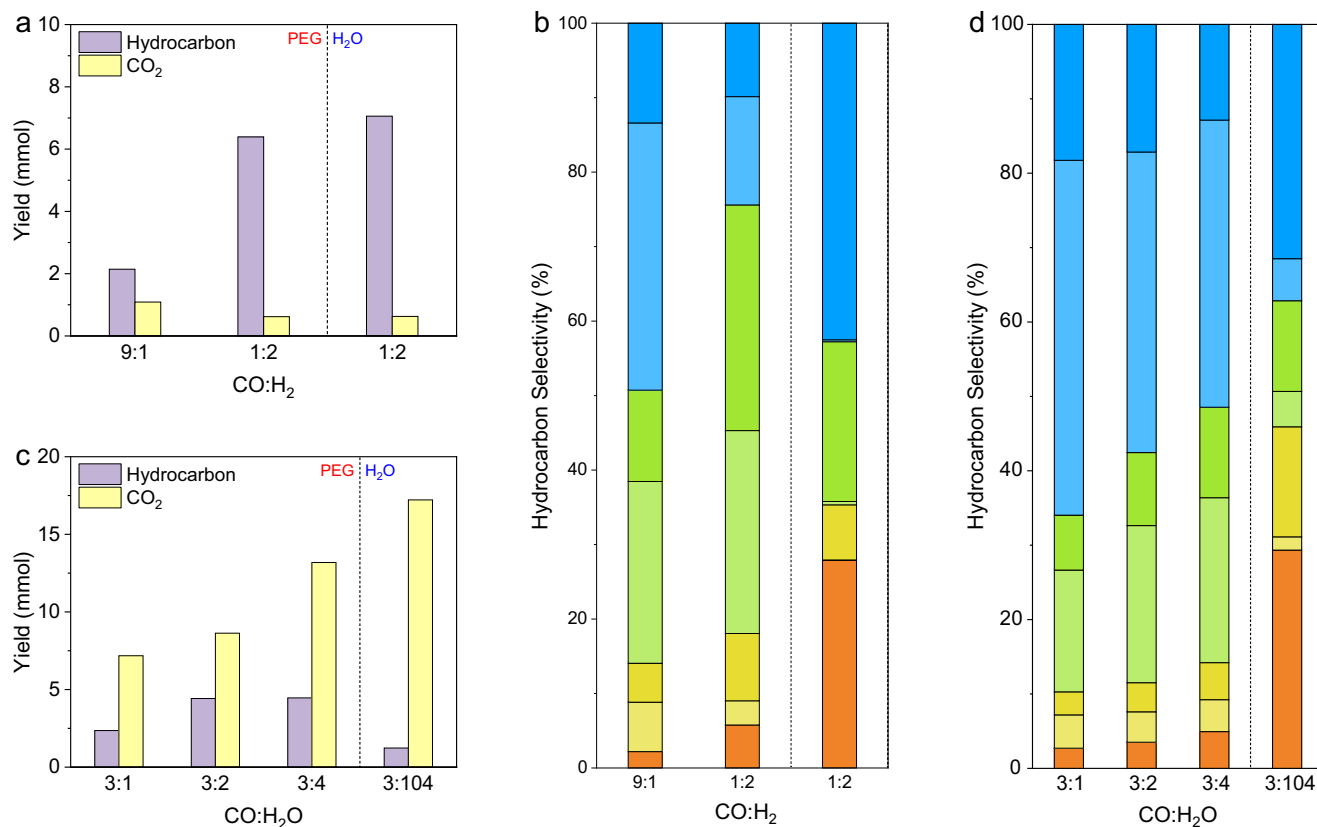


**Fig. 4 | Mechanistic studies on KES.** **a**, **b** FTS Catalytic performances for different ratios. **a** Yields of hydrocarbons and CO<sub>2</sub> on a carbon-atom basis. From left to right: CO/H<sub>2</sub> = 9:1 in PEG, CO/H<sub>2</sub> = 1:2 in PEG, and CO/H<sub>2</sub> = 1:2 in water. **b** Fractional hydrocarbon selectivity. From left to right: CO/H<sub>2</sub> = 9:1 in PEG, CO/H<sub>2</sub> = 1:2 in PEG, and CO/H<sub>2</sub> = 1:2 in water. All catalytic experiments were conducted in a 50-mL Hastelloy slurry reactor over Ru particles at 200 °C under 2 MPa of syngas for 10 h. Volume of solvent (pure water or PEG) was kept to 15 mL. **c**, **d** Impact of water on KES catalytic performances. **c** Yields of hydrocarbons and CO<sub>2</sub> on a carbon-atom

basis. From left to right: molar ratios of CO to H<sub>2</sub>O of 3:1, 3:2, 3:4, and 3:104 (water as the solvent). **d** Fractional hydrocarbon selectivity. From left to right: molar ratios of CO to H<sub>2</sub>O of 3:1, 3:2, 3:4 (PEG-400 as the solvent), and 3:104 (water as the solvent). Colors in panels **b** and **d** represent the same products as those in Fig. 3b. All catalytic experiments were conducted in a 50-mL Hastelloy slurry reactor over Pt/Mo<sub>2</sub>N-Ru at 200 °C under 2 MPa of CO for 10 h. Total volume of solvent (pure water for CO:H<sub>2</sub>O ratio of 3:104 or PEG solvent with 142, 284, and 568 μL of water for CO:H<sub>2</sub>O ratio of 3:1, 3:2, and 3:4, respectively) were kept to 15 mL.

aforementioned KES experiments, limiting amount of water, though tightly coupled with CO pressure, played a vital role in the yield of C<sub>12+</sub><sup>+</sup> (Supplementary Table S1). We conducted catalytic tests over Pt/Mo<sub>2</sub>N-Ru with pure water and different amounts of water in PEG solvent under 2 MPa of CO at 200 °C for 10 h. When the solvent was changed from PEG to pure water, an extreme CO:H<sub>2</sub>O ratio of 3:104 was obtained. As expected, the yield of CO<sub>2</sub> grew as the amount of water increased (Fig. 4c). The yield of hydrocarbons exhibited a volcano-type trend where the yield rose from 2.36 mmol (CO:H<sub>2</sub>O = 3:1) to 4.42 mmol (CO:H<sub>2</sub>O = 3:2) and 4.46 mmol (CO:H<sub>2</sub>O = 3:4) but finally descended to 1.23 mmol (CO:H<sub>2</sub>O = 3:104) (Fig. 4c, Supplementary Table S1). As shown in Fig. 4d, the distribution of hydrocarbons was sensitive to the amount of water. A high CO:H<sub>2</sub>O ratio resulted in a high CO:H<sub>2</sub> ratio, favoring both chain propagation and olefin formation. Hence, the C<sub>12+</sub><sup>+</sup> selectivity among hydrocarbons with the highest CO:H<sub>2</sub>O ratio of 3:1 reached the highest value of 47.7% (Supplementary Table S1). Supplementary Figure S12 shows the detailed hydrocarbon selectivity with CO:H<sub>2</sub>O ratios of 3:1, 3:4, and 3:104. Hydrocarbon distribution *via* KES in water was similar to that *via* FTS in water, with methane as major product. Only a small amount of olefins was formed with an o/p ratio of 0.21. Notably, the highest C<sub>12+</sub><sup>+</sup> yield (1.79 mmol) was still achieved under the CO:H<sub>2</sub>O ratio of 3:2. Effect of water on the hydrocarbon distribution over a constant pressure of 2 MPa ulteriorly corroborated the cause of the abnormal pressurization effect on hydrocarbon production (Fig. 3b).

The amounts of Pt/Mo<sub>2</sub>N and Ru particles also influenced the rates for WGS and FTS (Supplementary Figs. S13–14). When we halved the amount of Pt/Mo<sub>2</sub>N, the total yield drastically dropped to less than half of that under optimal condition. The amounts of Ru did not significantly affect the FTS process. We speculated that a certain amount of hydrogen was necessary to trigger and drive FTS, probably due to the rapid diffusion of produced hydrogen out of PEG and thus the limited activation over Ru. With double amount of Pt/Mo<sub>2</sub>N, elevated yield of CO<sub>2</sub> was observed. For a fixed reaction condition, merely increasing the rate of WGS could induce a mismatch of WGS and FTS, as we discussed above, while the yield of hydrocarbon exhibited a more sensitive dependence on Ru amounts than that at a low conversion.

The influence of the PEG molecular weight on the catalytic performance was explored (Supplementary Figs. S15, 16). Total yield was slightly higher in PEG-200 and severely restricted in PEG-600, due to the increasing viscosity with the increasing molecular weight. Though hydrocarbon yields, which were not as high as that in PEG-400, followed the trend discussed above, olefin-preference was still observed in PEG with different molecular weights.

Stability of this proposed system was also a necessity for practical application. However, Ru particles floating in viscous PEG phase during the extraction process led to the difficulty in separation of active components (Supplementary Fig. S17), and thus the stability test with multiple rounds. A *quasi*-stability test by studying the evolution of products for different reaction time became our alternative approach. With the prolonged reaction time, the yield of CO<sub>2</sub> continuously

increased at a diminishing rate due to the consumption of both CO and water, whereas the production of hydrocarbons steadily grew (Supplementary Fig. S18). The o/p ratio (for all C<sub>2+</sub> products) increased from 1.00 for 2.5 h to 2.13 for 10 h (Supplementary Table S1). Chain propagation was also favored for longer reaction time, evidenced by the increasing selectivity for C<sub>5+</sub> hydrocarbons over time (Supplementary Fig. S19). Detailed hydrocarbon selectivities for 2.5, 5, and 7.5 h are shown in Supplementary Fig. S20a–c. We ascribed the decreasing WGS rate to the consumption of CO and accumulation of CO<sub>2</sub> in gas instead of rapid deactivation. Otherwise, the yield of CO<sub>2</sub> should undergo a cliff drop. A restricted FTS rate was also observed at the initial stage, consistent with our observation of the results with half the amount of Pt/Mo<sub>2</sub>N (Supplementary Fig. S13). The XRD pattern and XPS spectra of the spent catalyst also suggested the structural stability of Mo<sub>2</sub>N and the metallic states of Pt and Ru (Supplementary Fig. S21). Hence, we speculated that stability during the reaction could be expected. The variation of C 1s spectrum was ascribed to that the formation of CH<sub>x</sub> on surface might expel PEG during the washing procedure. The Ru 3d<sub>5/2</sub> peak did not exhibit a measurable shift, compared with the fresh Pt/Mo<sub>2</sub>N-Ru sample with PEG residue, indicating PEG did not serve as an electronic promoter for Ru.

On account of the proof-of-concept nature of our strategy, we also extended our catalysts to non-noble metals to address the concern about the use of noble metals. It is generally accepted that Cu/ZnO/Al<sub>2</sub>O<sub>3</sub> (CZA) serves as an efficient WGS catalyst<sup>35,36</sup>, while Co/Al<sub>2</sub>O<sub>3</sub> is regarded as an active FTS catalyst. We physically mixed CZA with Co/Al<sub>2</sub>O<sub>3</sub> for the KES reaction at 240 °C under 3 MPa of CO in comparison with standalone CZA or Co/Al<sub>2</sub>O<sub>3</sub>. CZA was only active towards WGS but inert towards FTS, resulting in the absence of hydrocarbons. As for Co/Al<sub>2</sub>O<sub>3</sub>, the WGS activity was rather poor (Supplementary Table S1). The insufficient hydrogen supply restrained the FTS process over Co/Al<sub>2</sub>O<sub>3</sub>, leading to low yields of hydrocarbons and especially C<sub>12+</sub><sup>+</sup> (Supplementary Table S1 and Figs. S23–24). Though the activity and C<sub>12+</sub><sup>+</sup> selectivity of CZA-Co/Al<sub>2</sub>O<sub>3</sub> were lower than those of Pt/Mo<sub>2</sub>N-Ru, the great matching of WGS and FTS was also achieved with an o/p ratio of 4.19, indicating the universality of our strategy to tune selectivity of paraffins to olefins. Besides, iron-based catalysts themselves are both WGS active in the phase of iron oxides and FTS active in the phase of iron carbides. To this end, we conducted KES experiments on Fe-based catalysts at 240 °C, a temperature considered hard for olefin desorption from iron surface<sup>37</sup>. The olefin-preference was observed in spite of excessive CO<sub>2</sub> production due to the strong WGS activity (Supplementary Table S1 and Fig. S25).

## Discussion

We showcased the potential of KES proceeded in a phase-transfer agent, PEG in our case, over Pt/Mo<sub>2</sub>N-Ru to produce extra-heavy olefins. KES provided continuously low hydrogen pressure, kinetically favoring the formation of olefins. PEG served as a selective extraction agent of olefins. Under an optimized condition, the kinetics of WGS and FTS were perfectly matched, as the yield ratio of CO<sub>2</sub> to hydrocarbons reached the theoretical minimum of 2. Meanwhile, C<sub>12+</sub><sup>+</sup> yield reached its maximum of 1.79 mmol. Apart from Pt/Mo<sub>2</sub>N-Ru, we also extended to non-noble catalysts, proving the universality of this strategy. Compared with energy-intensive wax cracking process (>400 °C), severe operation conditions are not indispensable for this energy efficient KES route. KES route also enables the direct production of C<sub>12+</sub><sup>+</sup>, circumventing the multi-step SHOP.

## Methods

### Chemicals and materials

(NH<sub>4</sub>)<sub>6</sub>Mo<sub>7</sub>O<sub>24</sub>·4H<sub>2</sub>O, H<sub>2</sub>PtCl<sub>4</sub>·6H<sub>2</sub>O, RuCl<sub>3</sub>·xH<sub>2</sub>O (Ru amount: ~37%), FeCl<sub>3</sub>·6H<sub>2</sub>O, Co(NO<sub>3</sub>)<sub>2</sub>·6H<sub>2</sub>O, cyclohexane, ethanol, ethylene glycol, polyethylene glycol-200 (PEG-200), polyethylene glycol-400 (PEG-400), polyethylene glycol-600 (PEG-600) were purchased from

Sinopharm Chemical Reagent Co., Ltd. (Shanghai, China). 1-dodecene was purchased from Shanghai Aladdin Biochemical Technology Co., Ltd. (Shanghai, China). Al<sub>2</sub>O<sub>3</sub> (catalyst support, high surface area, 1/8 pellets) was purchased from Alfa Aesar(China) Chemicals Co., Ltd. (Shanghai, China). NH<sub>3</sub>, N<sub>2</sub>, CO (with 5% N<sub>2</sub> as the internal standard), CO<sub>2</sub>, H<sub>2</sub>, propylene, and syngas (H<sub>2</sub>:CO:Ar =64:32:4) were purchased from Nanjing Special Gas Factory Co., Ltd. (Nanjing, China). Syngas (H<sub>2</sub>:CO:N<sub>2</sub> = 9.6:85.1:4.3) was compounded manually. Propylene-containing syngas (H<sub>2</sub>:CO:C<sub>3</sub>H<sub>6</sub> = 14:14:2) was compounded manually. 50-mL Hastelloy slurry reactors were purchased from Shanghai Yanzheng Experiment Instrument Co., Ltd. (Shanghai, China).

### Synthesis of Mo<sub>2</sub>N

Typically, (NH<sub>4</sub>)<sub>6</sub>Mo<sub>7</sub>O<sub>24</sub>·4H<sub>2</sub>O was calcined at 500 °C for 6 h in a muffle furnace to obtain MoO<sub>3</sub>. MoO<sub>3</sub> was then nitrided in 1 bar of pure NH<sub>3</sub> flow with a flow rate of 50 mL min<sup>-1</sup> in a tube furnace. The tube was heated with a heating ramp rate of 5 °C min<sup>-1</sup> to 500 °C, and then a rate of 1 °C min<sup>-1</sup> to 750 °C. After being maintained at 750 °C for 9 h, the sample was naturally cooled to room temperature, followed by passivation in 1 bar of CO<sub>2</sub> flow with a flow rate of 50 mL min<sup>-1</sup> for 1 h.

### Synthesis of Pt/Mo<sub>2</sub>N

500 mg of Mo<sub>2</sub>N was dispersed in 200 mL of ethanol. 40 mL of H<sub>2</sub>PtCl<sub>4</sub>·6H<sub>2</sub>O aqueous solution (0.00128 mol L<sup>-1</sup>) and 40 mL of NaBH<sub>4</sub> ethanol solution (0.0102 mol L<sup>-1</sup>) were added dropwise with stirring into Mo<sub>2</sub>N suspension simultaneously with a rate of 20 mL h<sup>-1</sup> through a two-channel syringe pump at room temperature. The as-synthesized sample was washed with ethanol thrice to remove the residual ions, followed by drying at 60 °C under vacuum.

### Synthesis of Pt/Mo<sub>2</sub>N-Ru

Typically, after 100 mg of Pt/Mo<sub>2</sub>N was dispersed in 15 mL of PEG-400/water binary solvent (with 142, 284, and 426 μL of water for CO:H<sub>2</sub>O ratio of 3:1, 3:2, and 3:4 respectively) in a 50-mL Hastelloy slurry reactor, 100 mg of RuCl<sub>3</sub>·xH<sub>2</sub>O was added with stirring. After the reactor was pressurized with H<sub>2</sub> (1.0 MPa) at room temperature, the reactor was heated to 150 °C, then kept for 5 h, and cooled down to room temperature. Samples with other ratios of Pt/Mo<sub>2</sub>N to Ru were synthesized similarly.

### Synthesis of Ru particles

100 mg of RuCl<sub>3</sub>·xH<sub>2</sub>O was added into 15 mL of PEG-400 in a 50-mL Hastelloy slurry reactor with stirring. After the reactor was pressurized with H<sub>2</sub> (1.0 MPa) at room temperature, the reactor was heated to 150 °C, then kept for 5 h, and cooled down to room temperature. For FTS conducted in water, the as-synthesized particles were washed with water thrice to remove the residual PEG, and then transferred into a reactor with 15 mL of water.

### Synthesis of Ru/Pt/Mo<sub>2</sub>N

200 mg of Pt/Mo<sub>2</sub>N was dispersed in 200 mL of ethanol. 50 mL of RuCl<sub>3</sub>·xH<sub>2</sub>O aqueous solution (4 mg mL<sup>-1</sup>) and 50 mL of NaBH<sub>4</sub> ethanol solution (0.128 mol L<sup>-1</sup>) were added dropwise with stirring into Pt/Mo<sub>2</sub>N suspension simultaneously with a rate of 25 mL h<sup>-1</sup> through a two-channel syringe pump at room temperature. The as-synthesized sample was washed with ethanol thrice to remove the residual ions, followed by drying at 60 °C under vacuum.

### Synthesis of Fe-based catalyst

10 mL of 2.4 M KBH<sub>4</sub> aqueous solution was added dropwise to 30 mL of 0.2 M FeCl<sub>3</sub>·6H<sub>2</sub>O ethylene glycol solution with a rate of 20 mL h<sup>-1</sup> through a syringe pump under an inert atmosphere of N<sub>2</sub>. A magnet was used to separate Fe precipitate from solution. The precipitate was washed by ethanol 8 times to avoid the oxidation and remove the possible K residue.

### Synthesis of Co/Al<sub>2</sub>O<sub>3</sub>

Co/Al<sub>2</sub>O<sub>3</sub> was prepared by impregnating Co(NO<sub>3</sub>)<sub>2</sub>·6H<sub>2</sub>O onto Al<sub>2</sub>O<sub>3</sub> powder, followed by hydrogen reduction at 600 °C for 5 h.

### Extraction of 1-dodecene

95 mg of 1-dodecene was dispersed into a centrifuge tube containing 15 mL of PEG-400. 2 mL of cyclohexane was then added at room temperature, followed by vigorous shaking for 1 min. For the water-aided extraction, 10 mL of water was added into the mixture of cyclohexane and PEG at room temperature, followed by vigorous shaking for 1 min. 1-dodecene dissolved in cyclohexane was determined by gas chromatograph (Shimadzu GC-2014).

### Catalytic tests

All FTS and KES reactions were carried out in a 50-mL Hastelloy slurry reactor.

For FTS conducted in PEG-400, after the reduction of RuCl<sub>3</sub>·xH<sub>2</sub>O, the reactor was washed with N<sub>2</sub> for 5 times to remove H<sub>2</sub> residual and then pressurized with 2 MPa of syngas (H<sub>2</sub>/CO = 2/1 or 1/9) at room temperature. For FTS conducted in water, after the Ru particles were washed with water and transferred into a reactor, the reactor was washed with N<sub>2</sub> for 5 times to remove air residual and then pressurized with 2 MPa of syngas (H<sub>2</sub>/CO = 2/1) at room temperature. For propylene hydroformylation conducted in PEG-400, after the reduction of RuCl<sub>3</sub>·xH<sub>2</sub>O, the reactor was washed with N<sub>2</sub> for 5 times to remove H<sub>2</sub> residual and then pressurized with 3 MPa of propylene-containing syngas (H<sub>2</sub>/CO/C<sub>3</sub>H<sub>6</sub> = 14/14/2) at room temperature.

For typical KES test over Pt/Mo<sub>2</sub>N-Ru, the reactor was washed with N<sub>2</sub> for 5 times after the synthesis of Pt/Mo<sub>2</sub>N-Ru (typically, 100 mg of Pt/Mo<sub>2</sub>N and -37 mg of Ru particles) or the addition of 137 mg of Ru/Pt/Mo<sub>2</sub>N to remove hydrogen or air residual. Then the reactor was pressurized with 2, 3, or 4 MPa of CO at room temperature. All solvents (pure water, or PEG/water binary solvent) were kept to 15 mL. 284, 426, and 568 μL of water were used for 2, 3, and 4 MPa of CO while CO:H<sub>2</sub>O ratio was kept to 3:2, 142, 284, 568, and 15,000 μL of water were used for CO:H<sub>2</sub>O ratio of 3:1, 3:2, 3:4, and 3:104 while the pressure of CO was kept to 2 MPa. Procedure of KES tests over other catalysts was similar.

For one specified catalytic condition, two reactors were used. For accurate quantitation of total CO<sub>2</sub> (gaseous CO<sub>2</sub> and dissolved CO<sub>2</sub>), one reactor was heated and connected to a sealed container with 20 mL of NaOH aqueous solution (3.0 mol L<sup>-1</sup>). After CO<sub>2</sub> was entirely absorbed, 50 mL of Ba(NO<sub>3</sub>)<sub>2</sub> aqueous solution (0.5 mol L<sup>-1</sup>) was added. The precipitated BaCO<sub>3</sub> was washed thrice and dried at 80 °C overnight. The dried sample was weighed to calculate the amount of formed CO<sub>2</sub>. For quantitation of other gaseous compositions (CO and gaseous C<sub>1-7</sub> hydrocarbons), the other reactor was connected to a gas chromatograph (Shimadzu GC-2014). CO and CH<sub>4</sub> were analyzed by using a carbon molecular sieve column (TDX-1) with a thermal conductivity detector (TCD). The conversion of CO was determined by the internal standard merely for reference since dissolution in PEG might obscure the quantitation, while the procedure of accurate quantitation of hydrocarbons was as follow. Gaseous hydrocarbons were analyzed using an Al<sub>2</sub>O<sub>3</sub> capillary column with a flame ionization detector (FID) and a PONA capillary column with an FID. After quantitation of gaseous products, a certain amount of cyclohexane (typically 2 mL) was added into the reactor without stirring. After carefully transferring the liquid components (cyclohexane and PEG phases) and solid components (WGS catalysts and FTS catalysts) into a centrifuge tube, 10 mL of water was then added followed by 1-min shaking. The lid of centrifuge tube should be pressed hard during shaking, to prevent the dissolved CO<sub>2</sub> to pop out of the centrifuge tube and cause the loss of products. Cyclohexane solution was injected into a vaporization chamber in GC and then analyzed using a PONA capillary column with an FID. CH<sub>4</sub> was taken as a reference bridge between TCD and FID.

Hydrocarbons were calculated on a carbon-atom basis.

The selectivity for hydrocarbon C<sub>n</sub>H<sub>m</sub> was obtained according to

$$C_nH_m \text{ selectivity} = \frac{nC_nH_m}{\sum_i iC_iH_m} \times 100\% \quad (4)$$

In Eq. (4), C<sub>n</sub>H<sub>m</sub> represents moles of individual hydrocarbon products. Other possible oxygenate products were under the detection limit. The carbon balance was over 95%.

### Characterizations

XRD patterns were recorded by using a Philips X'Pert Pro Super diffractometer with Cu-Kα radiation (λ = 1.54178 Å). XPS measurements were conducted on an ESCALAB 250 (Thermo-VG Scientific, USA) with an Al Kα X-ray source (1486.6 eV photons) in Constant Analyser Energy (CAE) mode with a pass energy of 30 eV for all spectra. ICP-AES (Atomscan Advantage, Thermo Jarrell Ash, USA) was used to determine the loading amount of Pt. TEM images were taken using a Hitachi H-7700 transmission electron microscope at an acceleration voltage of 100 kV. HAADF analysis was collected on a Titan Themis Z transmission electron microscope with double aberration.

### Data availability

The data that support the findings of this study are available from the corresponding author upon reasonable request. Source data are provided with this paper.

### References

1. Corma, A. Inorganic solid acids and their use in acid-catalyzed hydrocarbon reactions. *Chem. Rev.* **95**, 559–614 (1995).
2. Keim, W. Oligomerization of ethylene to α-olefins: discovery and development of the shell higher olefin process (SHOP). *Angew. Chem. Int. Ed.* **52**, 12492–12496 (2013).
3. Yu, X. Q. et al. Preparation of α-olefins through the steam cracking process of wax from coal liquefaction. *Petrol. Sci. Technol.* **32**, 1291–1299 (2014).
4. Xu, Y. et al. A hydrophobic FeMn@Si catalyst increases olefins from syngas by suppressing C1 by-products. *Science* **371**, 610–613 (2021).
5. Zhao, B. et al. Direct transformation of syngas to aromatics over Na-Zn-Fe<sub>5</sub>C<sub>2</sub> and hierarchical HZSM-5 tandem catalysts. *Chem* **3**, 323–333 (2017).
6. Li, J. et al. Integrated tuneable synthesis of liquid fuels via Fischer-Tropsch technology. *Nat. Catal.* **1**, 787–793 (2018).
7. Peng, X. et al. Impact of hydrogenolysis on the selectivity of the Fischer-Tropsch synthesis: diesel fuel production over mesoporous zeolite-Y-supported cobalt nanoparticles. *Angew. Chem. Int. Ed.* **54**, 4553–4556 (2015).
8. Torres Galvis, H. M. et al. Supported iron nanoparticles as catalysts for sustainable production of lower olefins. *Science* **335**, 835–838 (2012).
9. Zhong, L. et al. Cobalt carbide nanoprisms for direct production of lower olefins from syngas. *Nature* **538**, 84–87 (2016).
10. Jiao, F. et al. Selective conversion of syngas to light olefins. *Science* **351**, 1065–1068 (2016).
11. Zhang, Y. et al. Tuning reactivity of Fischer-Tropsch synthesis by regulating TiO<sub>x</sub> overlayer over Ru/TiO<sub>2</sub> nanocatalysts. *Nat. Commun.* **11**, 3185 (2020).
12. Xiao, C., Cai, Z., Wang, T., Kou, Y. & Yan, N. Aqueous-phase Fischer-Tropsch synthesis with a ruthenium nanocluster catalyst. *Angew. Chem. Int. Ed.* **47**, 746–749 (2008).
13. Chen, J. & Liu, Z.-P. Origin of selectivity switch in Fischer-Tropsch synthesis over Ru and Rh from first-principles statistical mechanics studies. *J. Am. Chem. Soc.* **130**, 7929–7937 (2008).
14. Kang, J. et al. Mesoporous zeolite-supported ruthenium nanoparticles as highly selective Fischer-Tropsch catalysts for the

- production of C<sub>5</sub>–C<sub>11</sub> isoparaffins. *Angew. Chem. Int. Ed.* **50**, 5200–5203 (2011).
15. Gao, J. et al. Effective control of  $\alpha$ -olefin selectivity during Fischer-Tropsch synthesis over polyethylene-glycol wrapped porous catalyst. *Catal. Commun.* **12**, 1466–1470 (2011).
  16. Chun, D. H. et al. Highly selective iron-based Fischer-Tropsch catalysts activated by CO<sub>2</sub>-containing syngas. *J. Catal.* **317**, 135–143 (2014).
  17. Larkins, F. P. & Khan, A. Z. Investigation of K obel-Engelhardt synthesis over iron-based catalysts. *Appl. Catal.* **47**, 209–227 (1989).
  18. Kikuchi, E., Machino, A., Itoh, H., Fujishiro, K. & Morita, Y. Hydrocarbon synthesis from CO and H<sub>2</sub>O on supported ruthenium catalysts. *J. Japan Pet. Inst.* **29**, 240–245 (1986).
  19. Yasushi, M., Masamichi, A., Nobukazu, O. & Etsuro, E. Kinetic and mechanistic studies on the K obel-Engelhardt reaction over an iron oxide catalyst. *Bull. Chem. Soc. Jpn* **57**, 667–672 (1984).
  20. Xu, Y. et al. Direct conversion of CO and H<sub>2</sub>O into liquid fuels under mild conditions. *Nat. Commun.* **10**, 1389 (2019).
  21. Yao, S. et al. Atomic-layered Au clusters on  $\alpha$ -MoC as catalysts for the low-temperature water-gas shift reaction. *Science* **357**, 389–393 (2017).
  22. Lin, L. et al. Low-temperature hydrogen production from water and methanol using Pt/ $\alpha$ -MoC catalysts. *Nature* **544**, 80–83 (2017).
  23. Zhang, X. et al. A stable low-temperature H<sub>2</sub>-production catalyst by crowding Pt on  $\alpha$ -MoC. *Nature* **589**, 396–401 (2021).
  24. Wei, Z. B. Z., Grange, P. & Delmon, B. XPS and XRD studies of fresh and sulfided Mo<sub>2</sub>N. *Appl. Surf. Sci.* **135**, 107–114 (1998).
  25. Yu, H. et al. Direct production of olefins from syngas with ultrahigh carbon efficiency. *Nat. Commun.* **13**, 5987 (2022).
  26. Zamora-Justo, J. A. et al. Polyethylene glycol-coated gold nanoparticles as DNA and atorvastatin delivery systems and cytotoxicity evaluation. *J. Nanomater.* **2019**, 5982047 (2019).
  27. Shetty, S. & van Santen, R. A. CO dissociation on Ru and Co surfaces: the initial step in the Fischer–Tropsch synthesis. *Catal. Today* **171**, 168–173 (2011).
  28. Fan, X.-B., Tao, Z., Xiao, C., Liu, F. & Kou, Y. Liquid-phase Fischer-Tropsch synthesis over Fe nanoparticles dispersed in polyethylene glycol (PEG). *Green Chem.* **12**, 795–797 (2010).
  29. Senthamizh, S. R., Nanthini, R. & Sukanyaa, G. The basic principle of phase-transfer catalysis, some mechanistic aspects and important applications. *Int. J. Sci. Tech. Res.* **1**, 61–63 (2012).
  30. Totten, G. E. & Clinton, N. A. Poly[ethylene glycol] derivatives as phase transfer catalysts and solvents for organic reactions. *Polym. Rev.* **28**, 293–337 (1988).
  31. Zecevic, J., Vanbutsele, G., de Jong, K. P. & Martens, J. A. Nanoscale intimacy in bifunctional catalysts for selective conversion of hydrocarbons. *Nature* **528**, 245–248 (2015).
  32. Pilot, I. A. W., van Santen, R. A. & Hensen, E. J. M. The optimally performing Fischer–Tropsch catalyst. *Angew. Chem. Int. Ed.* **53**, 12746–12750 (2014).
  33. Pilot, I. A. W., van Santen, R. A. & Hensen, E. J. M. Quantum chemistry of the Fischer-Tropsch reaction catalysed by a stepped ruthenium surface. *Catal. Sci. Technol.* **4**, 3129–3140 (2014).
  34. Cheng, J. et al. Chain growth mechanism in Fischer-Tropsch synthesis: a DFT study of C-C coupling over Ru, Fe, Rh, and Re surfaces. *J. Phys. Chem. C* **112**, 6082–6086 (2008).
  35. Guo, P. et al. Cu/ZnO/Al<sub>2</sub>O<sub>3</sub> water-gas shift catalysts for practical fuel cell applications: the performance in shut-down/start-up operation. *Int. J. Hydrogen Energ.* **34**, 2361–2368 (2009).
  36. Zhang, Z. et al. The active sites of Cu-ZnO catalysts for water gas shift and CO hydrogenation reactions. *Nat. Commun.* **12**, 4331 (2021).
  37. Wang, C. et al. Fischer-Tropsch synthesis to olefins boosted by MFI zeolite nanosheets. *Nat. Nanotechnol.* **17**, 714–720 (2022).

## Acknowledgements

This work was supported by the National Key Research and Development Program of China (2021YFA1500500, 2019YFA0405600), CAS Project for Young Scientists in Basic Research (YSBR-051), National Science Fund for Distinguished Young Scholars (21925204), NSFC (U19A2015, 22221003, 22250007), Fundamental Research Funds for the Central Universities, Provincial Key Research and Development Program of Anhui (202004a05020074), K. C. Wong Education (GJTD-2020-15), the DNL Cooperation Fund, CAS (DNL202003), China Postdoctoral Science Foundation (2020M682007), China Postdoctoral Program for Innovative Talents (BX20200323), Natural Science Foundation of Anhui Province (2208085QB42), Collaborative Innovation Program of Hefei Science Center, CAS (2022HSC-CIP004), the joint Fund of the Yulin University and the Dalian National Laboratory for Clean Energy (YLU-DNL Fund 2022012) and USTC Research Funds of the Double First-Class Initiative (YD9990002014). This work was partially carried out at the USTC Center for Micro and Nanoscale Research and Fabrication.

## Author contributions

C.W. and J.D. equally contributed to this work. C.W., J.D., H.L., and J.Z. conceived the ideas and wrote the paper. C.W., J.D., and L.Z. synthesized catalysts. C.W., J.D., H.L., Z.P., and W.W. performed catalytic tests. C.W., Z.L., Y.D., and X.L. conducted characterizations. All authors discussed the results and commented on the manuscript.

## Competing interests

The authors declare no competing interests.

## Additional information

**Supplementary information** The online version contains supplementary material available at <https://doi.org/10.1038/s41467-023-37599-2>.

**Correspondence** and requests for materials should be addressed to Hongliang Li or Jie Zeng.

**Peer review information** *Nature Communications* thanks Abhishek Dutta Chowdhury and the other, anonymous, reviewers for their contribution to the peer review of this work.

**Reprints and permissions information** is available at <http://www.nature.com/reprints>

**Publisher's note** Springer Nature remains neutral with regard to jurisdictional claims in published maps and institutional affiliations.

**Open Access** This article is licensed under a Creative Commons Attribution 4.0 International License, which permits use, sharing, adaptation, distribution and reproduction in any medium or format, as long as you give appropriate credit to the original author(s) and the source, provide a link to the Creative Commons license, and indicate if changes were made. The images or other third party material in this article are included in the article's Creative Commons license, unless indicated otherwise in a credit line to the material. If material is not included in the article's Creative Commons license and your intended use is not permitted by statutory regulation or exceeds the permitted use, you will need to obtain permission directly from the copyright holder. To view a copy of this license, visit <http://creativecommons.org/licenses/by/4.0/>.

  The Author(s) 2023